Alteration and Non-formula Elements Uptake of Zircon From Um Ara Granite, South Eastern Desert, Egypt

Hamdy Hamed Abd El-Naby *

Posted Date: 16 July 2024

doi: 10.20944/preprints202407.1284.v1

Keywords: Zircon; non-formula elements; hydrothermal alteration; low-T alteration; Um Ara granite

Article

Alteration and Non-Formula Elements Uptake of Zircon from Um Ara granite, South Eastern Desert, Egypt

Hamdy H. Abd El-Naby *

King Abdulaziz University, Faculty of Earth Sciences, P.O. Box 80206 Jeddah 21589, KSA.
* Correspondence: hhabdel@yahoo.com; Mobile: 00966-549569066, Fax: 00966 12 6952441.

Abstract: The Um Ara granites are a suite of granitoid rocks located in the south Eastern Desert of Egypt. The combination of Back Scattered Electron imaging (BSE), X-ray compositional mapping, and the data of the Electron Probe Micro Analyzer (EPMA) has provided valuable insights into the alteration process of zircon in the Um Ara granite. The investigated zircon grains have measurable amount of non-formula elements such as U, Th, Hf, REEs, P, Al, Ca, Fe, and Ti, along with extensive structural features indicative of radiation damage. These characteristics point to significant hydrothermal alteration of the zircon following its initial crystallization. The textural and geochemical evidence suggests the alteration of the Um Ara zircons was driven by coupled dissolution-reprecipitation processes influenced by aqueous fluids. The breakdown of accessory minerals like xenotime, thorite, monazite, and apatite during a major hydrothermal event around 1.8 Ga released the non-formula elements (U, Th, P, Ca, Al, Fe, REEs) that were then incorporated into the zircon structures. Subsequent pluvial periods around 50,000-159,000 years ago may have allowed further uptake of these elements during low-temperature alteration. The shear zones within the Um Ara granites facilitated the mobilization and transport of the non-formula element-bearing fluids, likely as carbonate and fluoride complexes. The temperature regime, with fluids remaining below 300 °C, was crucial in preserving the radiation damage features in the zircons despite the extensive chemical changes.

Keywords: Zircon; Non-formula elements; Hydrothermal alteration; low-T alteration; Um Ara granite

1. Introduction

While zircon is generally considered a refractory mineral, it can undergo fluid-assisted alteration under different P-T conditions in the Earth's crust. Metamict zircon, in particular, exhibits enhanced reactivity towards fluids due to its amorphous or disrupted crystal lattice structure. Several studies have indicated that metamict zircon is predominantly affected by fluid- aided alteration, even under fairly low P-T conditions (Geisler et al., 2007; Lenting et al., 2010; Lewerentz et al., 2019). Metamict zircon, with its amorphous or disturbed crystal lattice, provides more accessible pathways for fluid infiltration and alteration than the original zircon. The susceptibility of zircon to fluid-assisted alteration can lead to changes in its mineralogical and chemical composition. This includes the incorporation or loss of certain elements as the fluid interacts with the zircon lattice. These alterations can have significant implications for interpreting geochronological, geochemical, and isotopic data obtained from zircon. A recent study by Harlov et al. (2023) highlights that even zircon with low levels of radiation fffect can undergo metasomatic alteration when exposed to alkali- and F-bearing solutions, which can induce chemical changes and modify the zircon structure. They demonstrate that zircon can be metasomatically altered under high P-T conditions within the lower crust. These solutions can induce chemical changes in zircon, leading to compositional modifications within the zircon structure.

During the initial stages of granite formation, zircon crystallizes from the magma as a durable and resistant mineral. The alteration of zircon is primarily driven by the introduction of hot

 doi:10.20944/preprints202407.1284.v1

hydrothermal fluids, which can mobilize elements, like U, Th, Hf, and rare earth elements (REEs), from the associated minerals, including zircon. These fluids facilitate the leaching of certain elements from zircon, particularly ZrO_2 and SiO_2. This leaching process can lead to partial to complete dissolution of zircon grains, leaving behind altered varieties. The composition of the hydrothermal fluids plays a crucial role in the alteration process. These fluids are often enriched in volatile components such as fluorine (F) and boron (B), which can be derived from the magmatic or metamorphic source rocks. Additionally, hydrothermal fluids may contain elevated concentrations of REEs and other trace elements such as U, Th, and Hf.

The zircon occurrence in the Um Ara area is associated with alkali-feldspar granites that were emplaced between 620 and 530 Ma and intruded the older metavolcanics and Dokhan volcanics. The study of zircon alteration is indeed a valuable approach for gaining insights into complex geological processes occurring in the Earth's crust. The researcher employed a multifaceted microanalytical approach to investigate various aspects of the zircon, including morphology, growth zoning, and compositional variations in major, trace, and REEs. This multi-technique analysis is crucial for elucidating the mechanisms and conditions of zircon alteration. The zircon from Um Ara exhibits a broad range of major element compositions, with low ZrO_2 and SiO_2 contents, along with high contents of "non-formula" elements such as U, Th, Fe, Al, Ca, P, Hf, As, and REEs. This research contributes to the broader understanding of the interplay between zircon alteration, fluid-mineral interactions, and the mobilization and concentration of valuable elements within the Earth's crust. Continued research in this field has the potential to yield further insights that can be applied across a range of geological disciplines, from mineralogy and petrology to geochemistry and geochronology.

2. Geological and Mineralogical Background

In the present study, zircon crystals have been examined from specimens collected from alkali-feldspar granites of the Um Ara area (Fig, 1). This area consists predominantly of granite intrusions that are associated with metavolcanics and Dokhan volcanics. Petrographically, these granites are classified as monzogranite and alkali-feldspar granite. Radiometric ages of the granitic rocks in the Um Ara area range between 589 Ma for monzogranite and 556 Ma for alkali feldspar granite (Abdalla et al., 1996). Despite the period of approximately 33 million years between the emplacement of the monzogranite and the alkali-feldspar granite, both granitic masses are considered part of the post-orogenic magmatic activity that occurred in the Egyptian shield between 620 and 530 Ma (Abdalla et al., 1996). The alkali-feldspar granites in particular have undergone late-stage hydrothermal alteration, as documented by Abdalla et al. (1996), and Abd El-Naby (2009). This hydrothermal alteration involves the mobilization and redistribution of high field strength elements, leading to the formation of new mineral assemblages and the replacement of pre-existing minerals within the granitic rocks.

 doi:10.20944/preprints202407.1284.v1

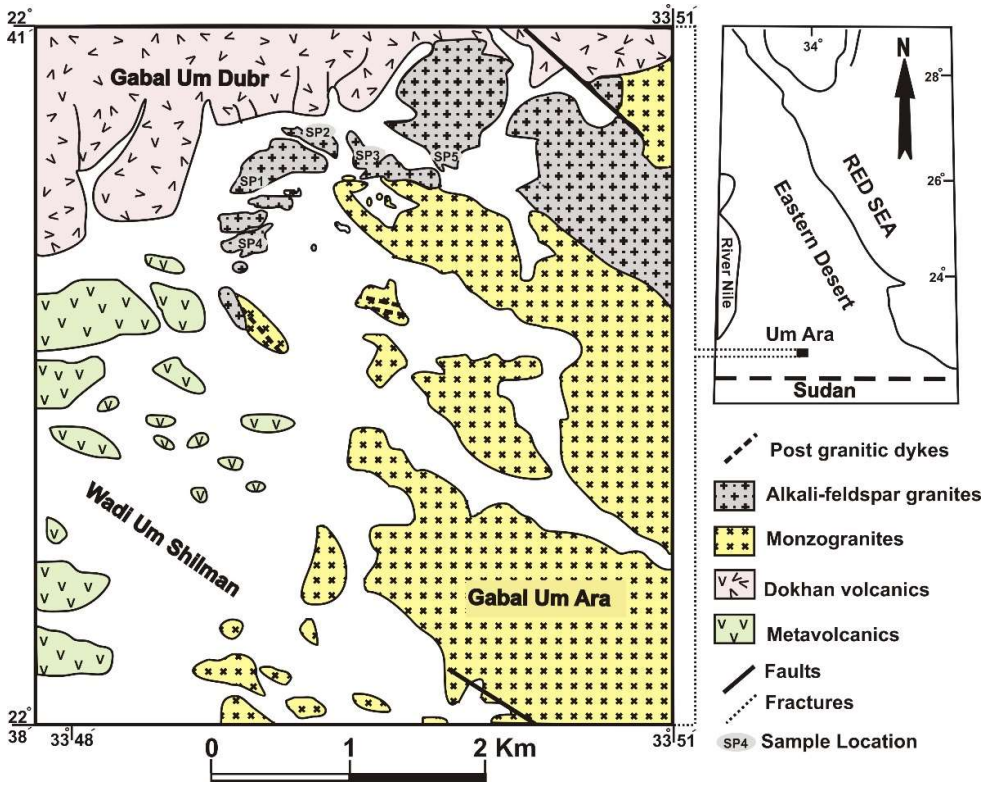

Figure 1. Geological map of Um Ara area (modified from Abdalla et al., 1996).

The investigated rock samples, collected from the alteration zones (K- and Na- metasomatism), consist of colourless to little brown and minute zircon crystals that show a pronounced variation in morphology and are commonly metamictized towards the core. Based on field observations and microscopic examinations of both reflected and transmitted light, it has been found that zircon is closely associated with disseminated xenotime, thorite, monazite, apatite, ilmenite, and uranophane. Uranophane occurs as yellow fine acicular crystals, that are assembled in fibrous masses. Prismatic to tabular crystals of thorite were recorded in association with zircon and other accessory minerals. Monazite occurs as brown rounded and fractured crystals. Fluorite of violet and colourless occurs as veinlets in the altered zone of the granitic rocks. Multiple stages of fluid activity, including both high-temperature hydrothermal fluids and lower-temperature meteoric waters, played a key role in the alteration and mineralization observed in the Um Ara granite. The interplay between these fluid-driven processes was a significant factor in the zircon alteration that occurred.

3. Analytical Procedures

Five samples were collected from the alkali feldspar granites of the Um Ara area at five different locations (Figure 1). The collected samples were initially washed with distilled water to remove any salts. The dried samples were crushed to the sand size fraction and then sieved using 500 μm, 250 μm, 125 μm, and 63 μm sieves. The fine and very fine sand sizes were combined in one fraction, and later subjected to heavy liquid separation using bromoform. The magnetite grains were removed from the heavy fractions by a hand magnet, with the remainder being split into four subfractions using a Frantz isodynamic separator at 0.2, 0.5, and 1.5 A. These subfractions were mounted on glass slides for mineral identification using a polarizing microscope. Mostly zircon grains were identified in the 1.5 A non-magnetic fraction. Several zircon grains from this fraction were hand-picked using a binocular reflected light microscope, mounted, and polished for further microprobe analyses. BSE, X-ray peak intensity mapping, and quantitative analyses of zircon grains and associated uranophane were performed on a JEOL JXA-8200 EPMA available at the Faculty of Earth Sciences, King Abdulaziz

 doi:10.20944/preprints202407.1284.v1

University, Saudi Arabia. The operating voltage is 20 kV, the beam diameter is 2-10 μm, and the beam current = 6–60 nA.

Fifty analyses on zircon and six analyses on the associated uranophane were performed, using natural and synthetic standards. Data reduction for the various elements was performed by taking into account the matrix corrections between standards and samples and the analytical parameters. The matrix effects were corrected by the conventional ZAF method which is employed by JEOL 8200 EPMA instrument. Any deviation from the initial, linear relation is 'corrected' by a series of multiplicative factors that account for the effects of atomic number (Z—stopping power, back-scattering factor, and X-ray production power), absorption (A) and fluorescence (F), each of which is calculated. The calculation of the sample detection limits is based on the standard counts, the unknown background counts, and includes the magnitude of the ZAF correction factor. The calculation is adapted from Scott et al. (1995). This detection limit in ppm is shown in Table 1 for each element with a confidence of 99% (assuming 3 standard deviations). Moreover, special care was taken to ensure that line overlaps were properly corrected and that background positions were clear of interfering lines among the REEs. The accuracy of unknown analyses was checked routinely by analyzing Lab standards as unknowns.

Table 1. Setup and operating conditions for EPMA analyses.

Element	Line	Std.	Crystal	Counting time (Sec.)	Limit Of Quantification (LOQ) (wt.%)
Si	Kα1	Wollastonite	PETH	10	0.066
Zr	Lα1	Zr oxide	PETJ	10	0.042
U	Mα1	UO_2	PETH	10	0.081
Th	Mα1	ThO_2	PETH	10	0.102
Hf	Lα1	HfO_2	LIFH	10	0.033
Pb	Mα1	PbVGe Oxides	PETH	10	0.015
Fe	Kα1	Fe_2O_3	LIFH	10	0.033
Al	Kα1	Y-garnet	TAP	10	0.027
Ca	Kα1	Wollastonite	PETJ	10	0.051
Mg	Kα1	MgO	TAP	10	0.051
Ti	Kα1	Ilmenite	PETJ	10	0.024
P	Kα1	$LaPO_4$	TAP	10	0.081
Y	Lα1	Y-garnet	TAP	10	0.039
AS	Lα1	Cal-STD	LIF	10	0.039
La	Lα1	$LaPO_4$	LIF	10	0.045
Ce	Lα1	$CePO_4$	LIFH	10	0.069
Nd	Lβ1	$NdPO_4$	LIFH	10	0.036
Sm	Lβ1	$SmPO_4$	LIFH	10	0.057
Eu	Lβ1	$EuPO_4$	LIFH	10	0.036
Gd	Lβ1	$GdPO_4$	LIF	10	0.075
Tb	Lβ1	$TbPO_4$	LIFH	10	0.036
Dy	Lβ1	$DyPO_4$	LIFH	10	0.075
Ho	Lβ1	$HoPO_4$	LIFH	10	0.018

 doi:10.20944/preprints202407.1284.v1

Er	Lβ1	$ErPO_4$	LIFH	10	0.018
Tm	Lα1	$TmPO_4$	LIFH	10	0.018
Yb	Lα1	$YbPO_4$	LIFH	10	0.039
Lu	Lα1	$LuPO_4$	LIFH	10	0.021

4. Results

4.1. Textural Observations

The zircon grains in the studied samples exhibit two distinct textural types. The first type is referred to as the zoned zircon grains (Figure 2c, Figure 3), which are the more prevalent type of zircon observed. They exhibit a distinct zonal texture, with a less altered core and a more altered outer rim. The contrast in BSE intensity between the inner and outer parts indicates different degrees of alteration. The more altered outer part of the zoned zircon is enriched in elements like Th, U, Hf, and REEs. Conversely, this outer altered part is depleted in Zr and Si compared to the less altered inner core (Figure 4). The less altered inner core has significantly lower concentrations of trace and rare earth elements compared to the outer region, but higher Zr and Si contents. The second type is referred to as the unzoned zircon grains, which exhibit mottled textures with numerous micropores (Figure 2a–d). The selective enrichment of the peripheries with elements like U, Th, Hf, and REEs points to a fluid-mediated alteration process that preferentially affected the grain boundaries and outer zones of the zircon crystals, while the core compositions remained relatively more pristine.

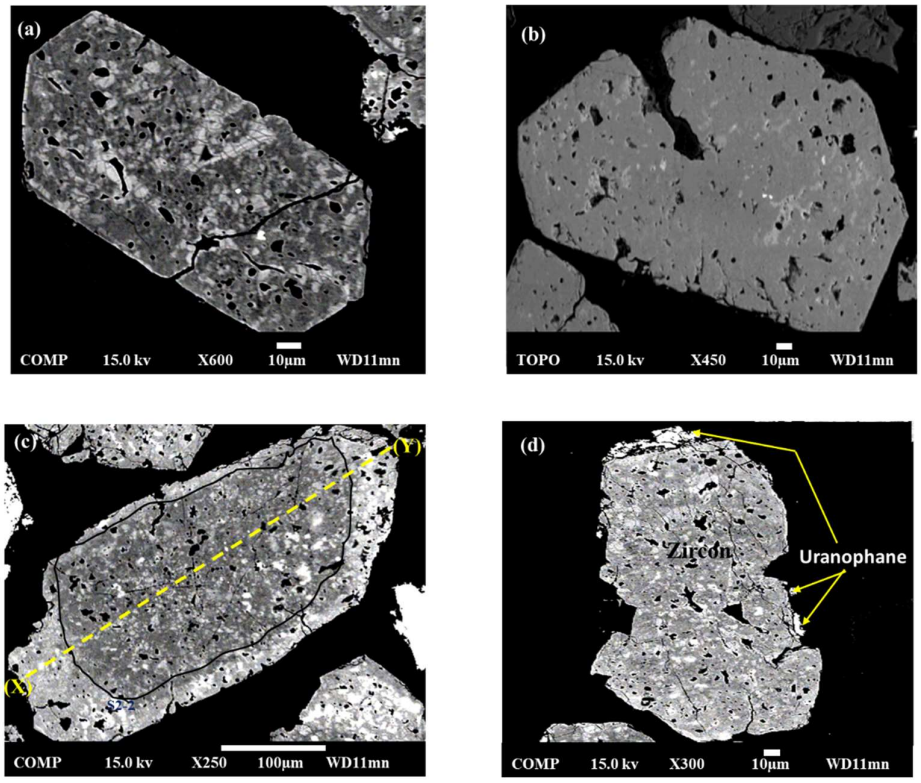

Figure 2. BSE imaging showing morphological characteristics of zircon grains separated from granites from of Um Ara area, south Eastern Desert of Egypt.

 doi:10.20944/preprints202407.1284.v1

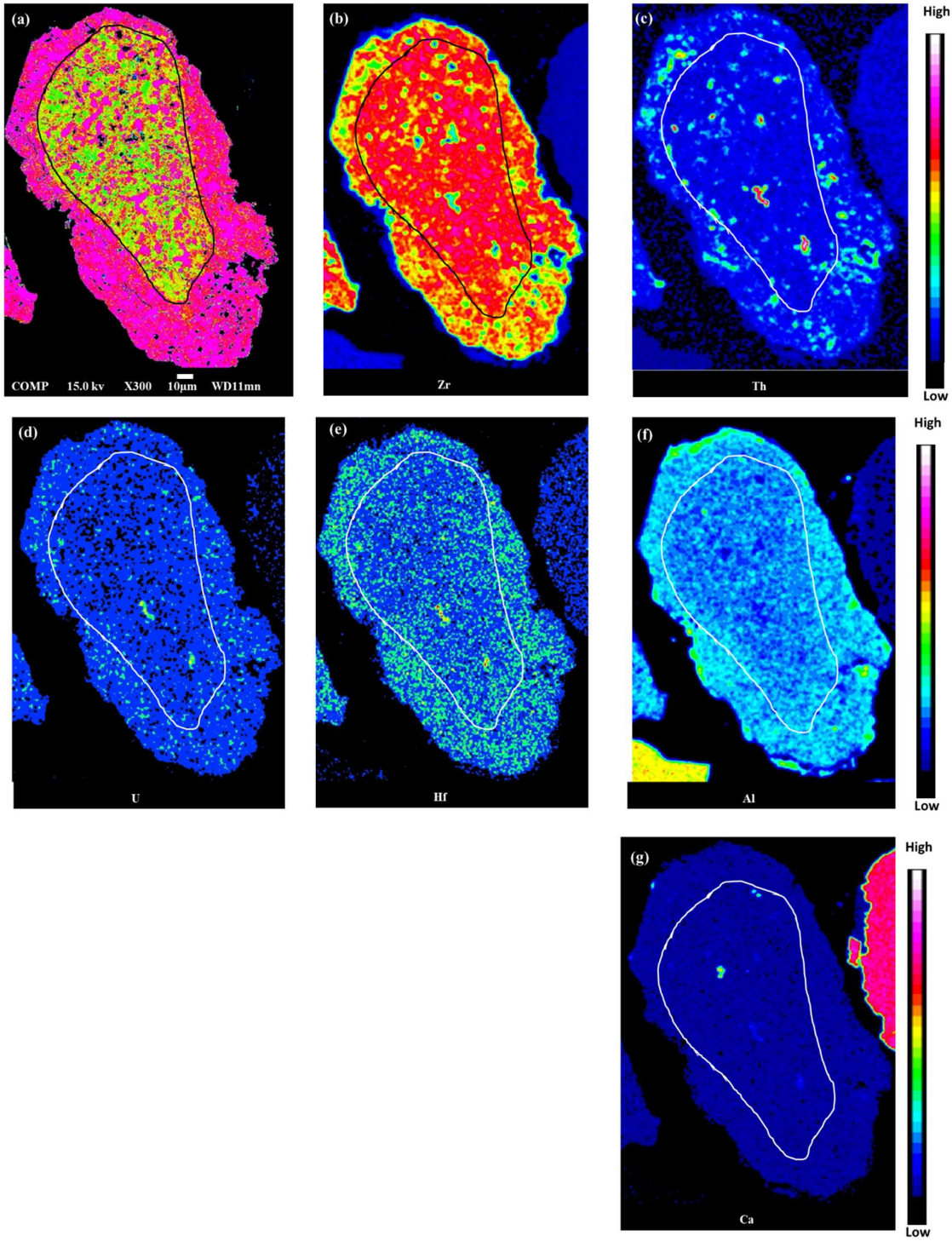

Figure 3. (a) False-colored peak intensity map showing zoning in zircon. **(b, c, d, e, f, g)** peak intensity mappings showing the distribution of Zr, Th, U, Hf, Al, and Ca in the grain of image **'a'**. Outer rims show a higher concentration of Th, U, Hf, and Al and a lower concentration of Zr.

 doi:10.20944/preprints202407.1284.v1

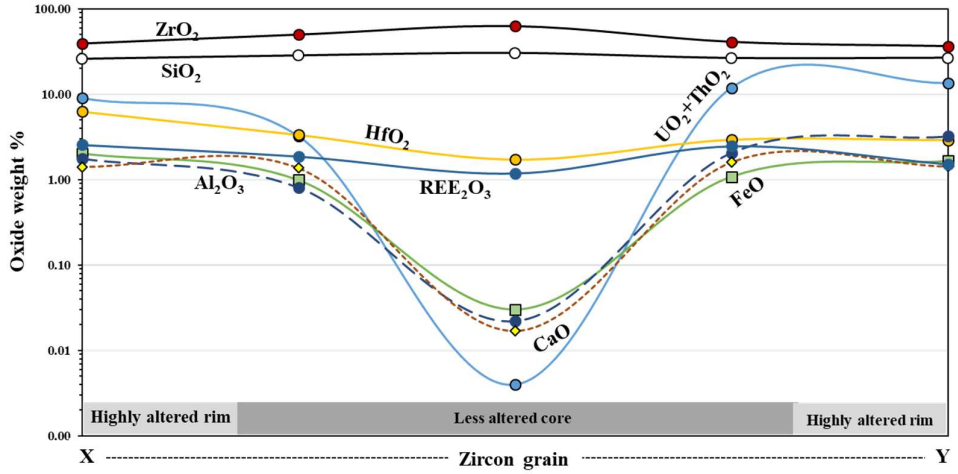

Figure 4. Analyses of the different sectors along the line X–Y in Figure **2c** reveal variations of SiO_2, ZrO_2, HfO_2, UO_2+ThO_2, Al_2O_3, FeO, CaO and REE_2O_3.

4.2. Major and Trace Elements Composition

The EPMA data (Table 2) reveals a bimodal distribution of zircon compositions, with a minor population of less altered zircons having major element totals close to 100 wt%, and a dominant group of more altered zircons with lower totals (ranging from 80 to 98 wt%). The decreasing ZrO_2 and SiO_2 contents with lower analytical totals suggest progressive alteration of the zircon grains, likely due to the mobilization and loss of major elements during the alteration process. Zircons with totals close to 100 wt% have ZrO_2 and SiO_2 contents close to the ideal end-member zircon composition (Figure 5a), indicating they are less altered. Across the entire dataset, both ZrO_2 and SiO_2 contents decrease linearly with decreasing analytical totals. This suggests that the zircon exhibits significant compositional variability. It has high and variable concentrations of "non-formula" elements, including HfO_2 (3.80 wt%, on average), ThO_2 (1.74 wt%, on average), UO_2 (1.24 wt%, on average), FeO (1.18 wt%, on average), Al_2O_3 (0.96 wt%, on average), CaO (1.00 wt%, on average), P_2O_5, (0.55 wt%, on average), Y_2O_3 (0.49 wt%, on average), TiO_2 (0.23 wt%, on average), and As_2O_3 (0.14 wt%, on average). In addition to a negligible amount of PbO (0.07 wt%, on average), and MgO (0.03 wt%, on average). Compared to the highly altered variety, the less altered variety is characterized by lower amounts of UO_2, ThO_2, PbO, FeO, Al_2O_3, CaO, MgO, TiO_2, P_2O_5, As_2O_3 concentrations, and higher ZrO_2, SiO_2 and Y_2O_3 concentrations, with REE below the detection limit.

Table 2. Representative EPMA analyses of zircon and associated uranophane from Um Ara alkali-feldspar granite.

Mineral type	**Less altered Zircon**				**Altered Zircon**				**Uranophane**	
Sample	**SP1**	**SP2-1**	**SP2-2**	**SP3-1**	**SP3-2**	**SP4-1**	**SP5**	**SP4-2B**	**U1**	**U3**
	(N*=1)	**(N*=2)**	**(N*=8)**	**(N*=7)**	**(N*=8)**	**(N*=8)**	**(N*=8)**	**(N*=8)**	**(N=3)**	**(N=3)**
					Oxides (wt.%)					
SiO_2	32.853	32.846	30.518	30.913	28.44	26.48	25.84	26.66	14.327	13.696
ZrO_2	66.273	64.848	63.184	62.605	50.04	41.08	39.2	36.52	0.037	0.006
UO_2	0.083	0.118	0.085	0.013	2.195	3.166	2.262	5.518	66.685	60.288
ThO_2	0.103	0.05	-	0.038	1.035	8.685	6.73	8.01	-	-
HfO_2	-	0.075	1.716	1.275	3.342	2.931	6.257	2.905	0.157	-
PbO	-	-	-		0.092	-	-	0.104	-	-
FeO	0.152	0.145	0.035	0.625	0.992	1.086	2.035	1.662	0.219	0.284

 doi:10.20944/preprints202407.1284.v1

Al_2O_3	-	-	0.029	-	0.813	2.062	1.768	3.224	0.15	0.289
CaO	0.057	0.043	-	0.051	1.368	1.597	1.416	1.426	6.764	6.143
MgO	-	-	-	-	0.059	0.055	-	0.074	0.029	0.069
TiO_2	-	-	0.053	0.064	0.026	-	-	-	0.014	-
P_2O_5	-	-	-	-	0.248	0.417	0.39	0.128	-	-
Y_2O_3	-	-	-	-	0.518	-	0.564	-	-	-
As_2O_3	-	-	-	-	0.06	0.061	0.22	0.128	0.034	0.055
La_2O_3	-	-	0.046	0.047	0.07	0.15	0.25	0.054	-	0.056
Ce_2O_3	-	-	0.079	0.07	0.103	1.024	0.941	0.856	0.183	-
Nd_2O_3	-	-	0.106	0.126	0.04	0.039	0.037	0.036	0.118	0.06
Sm_2O_3	-	-	0.059	0.075	0.063	0.184	0.144	0.066	-	-
EU_2O_3	-	-	0.056	0.091	0.04	0.037	0.038	0.045	-	-
Gd_2O_3	-	-	0.198	0.175	0.081	0.164	0.11	0.078	-	-
Tb_2O_3	-	-	0.037	0.037	0.037	0.039	0.037	0.039	-	0.089
Dy_2O_3	-	-	0.077	0.162	0.288	0.328	0.177	0.241	-	-
Ho_2O_3	-	-	0.175	0.104	0.082	0.02	0.018	0.018	-	-
Er_2O_3	-	-	0.02	0.02	0.356	0.053	0.413	0.076	-	-
Tm_2O_3	-	-	0.062	0.023	0.193	0.018	0.037	0.072	-	0.035
Yb_2O_3	-	-	0.26	0.078	0.489	0.393	0.395	0.044	-	-
Lu_2O_3	-	-	0.112	0.033	0.182	0.089	0.03	0.021	-	0.075
Total	99.52	98.13	96.91	96.56	91.25	90.16	89.31	88.01	88.72	81.15

Table 2. continued.

Mineral type	**Less altered Zircon**				**Altered Zircon**				**Uranophane**	
Sample	**SP1 (N*=1)**	**SP2-1 (N*=2)**	**SP2-2 (N*=8)**	**SP3-1 (N*=7)**	**SP3-2 (N*=8)**	**SP4-1 (N*=8)**	**SP5 (N*=8)**	**SP4-2B (N*=8)**	**U1 (N=3)**	**U3 (N=3)**
Structural formula	**Based on O = 4**								**Based on O = 7**	
Si	1.0065	1.0167	0.9816	0.9908	0.9912	0.9757	0.9688	1.0001	1.5076	1.5490
Al	-	-	0.0008	-	0.0334	0.0895	0.0781	0.1424	0.0186	0.0385
P	-	-	-	-	0.0073	0.0130	0.0124	0.0041	-	-
As	-	-	-	-	0.0013	0.0014	0.0050	0.0029	0.0022	0.0038
T-site	1.0065	1.0167	0.9824	0.9908	1.0332	1.0796	1.0643	1.1495		
Zr	0.9900	0.9788	0.9910	0.9785	0.8504	0.7381	0.7167	0.6680	0.0019	0.0003
U	0.0006	0.0008	0.0006	0.0001	0.0170	0.0260	0.0189	0.0461	1.5616	1.5174
Th	0.0007	0.0004	-	0.0003	0.0082	0.0728	0.0574	0.0684	-	-
Hf	-	0.0007	0.0158	0.0117	0.0332	0.0308	0.0670	0.0311	0.0047	-
Pb	-	-	-	-	0.0009	0.0001	-	0.0011	-	-
Fe	0.0039	0.0038	0.0008	0.0168	0.0289	0.0335	0.0638	0.0521	0.0193	0.0269
Ca	0.0006	0.0014	-	0.0018	0.0511	0.0630	0.0569	0.0573	0.7626	0.7444

 doi:10.20944/preprints202407.1284.v1

Mg	-	-	-	-	0.0031	0.0009	-	0.0041	0.0045	0.0116
Ti	-	-	0.0013	0.0015	0.0001	-	-	-	0.0011	-
Y	-	-	-	0.0000	0.0096	-	0.0112	-	-	-
La	-	-	0.0004	0.0004	0.0009	0.0020	0.0035	0.0002	-	0.0023
Ce	-	-	0.0007	0.0005	0.0013	0.0138	0.0129	0.0117	0.0070	-
Nd	-	-	0.0012	0.0014	0.0002	0.0002	0.0002	0.0005	0.0044	0.0024
Sm	-	-	0.0007	0.0008	0.0004	0.0023	0.0019	0.0009	-	-
Eu	-	-	0.0006	0.0003	0.0002	0.0002	0.0002	0.0002	-	-
Gd	-	-	0.0021	0.0010	0.0002	0.0020	0.0014	0.0010	-	-
Tb	-	-	0.0003	0.0003	0.0003	0.0004	0.0002	0.0002	-	0.0033
Dy	-	-	0.0001	0.0002	0.0032	0.0039	0.0021	0.0029	-	-
Ho	-	-	0.0018	0.0017	0.0009	0.0001	0.0002	0.0002	-	-
Er	-	-	0.0001	0.0001	0.0039	0.0006	0.0049	0.0009	-	-
Tm	-	-	0.0006	0.0001	0.0021	0.0001	0.0004	0.0008	-	0.0012
Yb	-	-	0.0025	0.0008	0.0052	0.0044	0.0045	0.0003	-	-
Lu	-	-	0.0011	0.0008	0.0019	0.0010	0.0003	0.0001	-	0.0026
A-Site	1.00	0.99	1.02	1.02	1.02	1.00	1.02	0.95		
Total	2.002	2.003	2.004	2.010	2.056	2.076	2.089	2.098	3.896	3.904

(–) means below detection limit.

 doi:10.20944/preprints202407.1284.v1

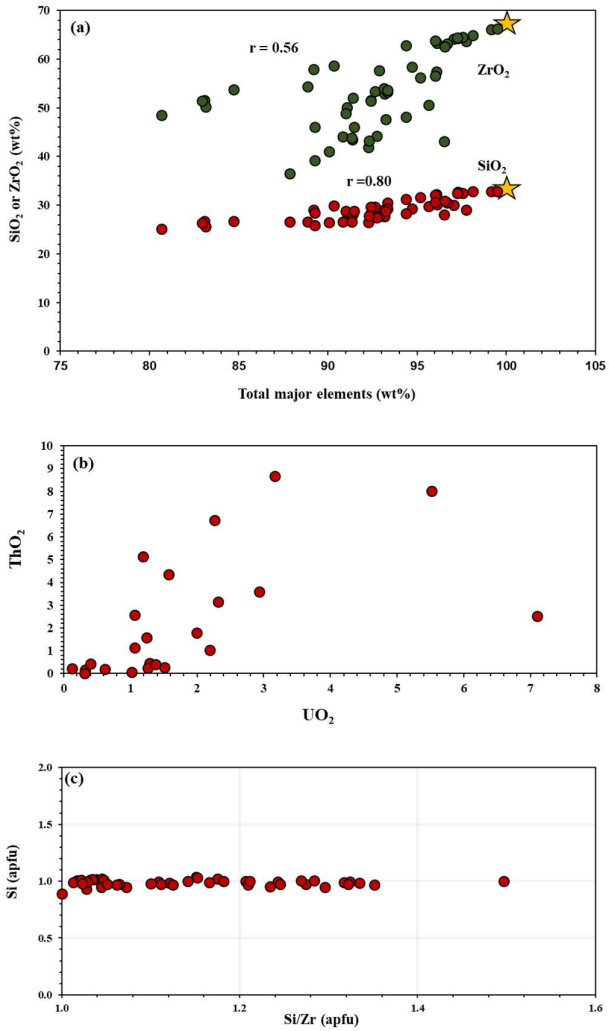

Figure 5. (a) Binary plot of total major elements (wt%) versus SiO_2 and ZrO_2 for the Um Ara zircon. Theoretical endmember pure zircon indicated by the orange asterisk (where total major elements = 100 wt%, SiO_2 = 32.8 wt%, and ZrO_2 = 67.2 wt%, Hoskin and Schaltegger, 2000). **(b)** Scattered relationship between UO_2 and ThO_2. **(c)** Si vs. Si/Zr bivariant plot of variably altered zircon grains.

From the scattered relationship between both actinides (Figure 5b), it could be concluded that some redistribution, including the loss or even gain of U and/or Th occurred. The presence of uranophane at the peripheries of zircon grains would indicate that a U-enriched fluid phase existed. This fluid is responsible on the enrichment of altered peripheries of zircon grains with U, Th, Hf, and REE. Despite the incorporation of non-formula elements (Th, U, Ca, P, Fe, Hf, Al, and REEs), the fundamental zircon structure was largely preserved, as evidenced by the consistent SiO_2/ZrO_2 ratio (Figure 5c).

4.3. REE Pattern of Zircon

Figure 6 shows the REE patterns of the altered zircons in comparison with the pattern of unaltered magmatic zircon as reported by Skublov et al. (2020). The REE distribution in the unaltered magmatic zircon shows a strong fractionation, with a steady increase from LREEs to HREEs and a moderately negative Eu anomaly (Figure 6). The studied altered zircon has an anomalously high REE content (Figure 6). The average LREE content of altered zircons is high (6155) ppm and the average HREE is higher than LREE (8582 ppm). The REE patterns of altered zircon is almost flat at the entire range (Lu_N/La_N averages 8.99). There is a positive Ce and Eu anomaly (Figure 6), with an average

 doi:10.20944/preprints202407.1284.v1

Eu/Eu* of 1.88. The $(La/Lu)_N$ ratio is less than 1 (averages 0.35). This suggests that the zircons experienced a secondary enrichment event that preferentially increased the LREE and HREE concentrations, resulting in a flat REE pattern. The positive Ce and Eu anomalies indicate oxidizing conditions during this alteration (Claiborne et al., 2010, Trail et al., 2012).

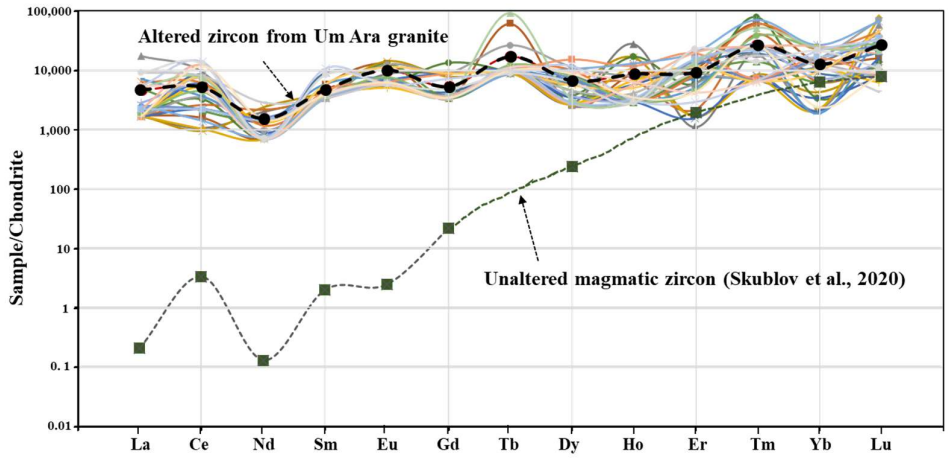

Figure 6. Rare earth element patterns of Um Ara altered zircon, normalized to the C1 chondrite values of McDonough and Sun (1995). The dashed black line represents the mean chondrite pattern of Um Ara altered zircon. The chondrite pattern of unaltered magmatic zircon is shown for comparison.

The average of the $(Sm/La)_N$ ratios observed in the studied altered zircons is 1.78. These ratios are significantly lower than the $(Sm/La)_N$ ratios typically observed in unaltered magmatic zircon, ranging from 33 to 653 (Hoskin, 2005). The La–Sm_N/La_N discrimination diagram (Figure 7) represents the compositions of porous, hydrothermal, and unaltered igneous zircons, as indicated by previous studies (Hoskin, 2005; Grimes et al., 2009; Bouvier et al., 2012). In this diagram, the studied zircon grains are located beyond the established compositional ranges, but close to the field of hydrothermal zircon. This positioning suggests that the parental zircon has undergone fluid-driven alteration, resulting in higher La contents (384–4093 ppm) and lower $(Sm/La)_N$ ratios (0.208–5.47) in the altered zircon. Furthermore, the REE patterns of the studied zircon indicate that the incorporation of dissolved REEs during a hydrothermal stage has led to substantial variations in the REE distribution compared to the parental zircon. In general, the altered zircon grains exhibit higher total REE concentrations than the unaltered magmatic zircon.

5. Discussion

5.1. Zircon Alteration

Zircon is widely recognized as a highly resistant and durable mineral. However, despite its renowned chemical and physical stability, zircon can experience remarkable structural and chemical modifications due to a variety of processes: a) over time, the emission and recoil of alpha particles can cause substantial structural changes within the zircon crystal (Murakami et al., 1991; Ewing et al., 2003; Marsellos and Garver, 2010). This radiation-induced damage can profoundly alter the internal structure of the mineral; b) deformation can also lead to the formation of internal microstructures within zircon grains. (Reddy et al., 2006). These deformation-related features can significantly modify the zircon's original structure; and c) interaction with hydrothermal fluids can result in the partial dissolution of the original zircon mineral. This is followed by the reprecipitation of new zircon material (Geisler et al., 2007; Soman et al., 2010; Seydoux-Guillaume et al., 2015). These various alteration processes—radiation damage, deformation, and hydrothermal alteration—can substantially alter the characteristics of zircon, despite its generally accepted reputation as a robust and durable mineral.

 doi:10.20944/preprints202407.1284.v1

The research conducted by Soman et al. (2010), Tomaschek et al. (2003), and Nasdala et al. (2009) provide further evidence for the involvement of alteration processes in zircon crystals. Soman et al. (2010) investigated the alteration effects on zircon crystals from an alkaline pegmatite in Malawi. They found that both interface-controlled and diffusion-controlled processes can operate simultaneously to modify the zircon. The participation of a fluid phase has been recognized in the formation of porous, inclusion-bearing zircon crystals from blueschist rocks in Greece (Tomaschek et al., 2003). The zircon crystals from these blueschist rocks contain mineral inclusions, such as xenotime and an unknown Y-REE-Th silicate phase. The presence of these mineral inclusions within the zircon indicates that fluid-mediated processes play a role in the alteration and formation of these inclusions. Furthermore, Nasdala et al. (2009) concluded that alteration domains observed in heavily radiation-damaged zircon grains contain water and exhibit a distinct microtexture and composition compared to pristine areas. This implies that water and other elements can diffuse into radiation-damaged zircon, triggering alteration processes that can lead to structural recovery or recrystallization, depending on the temperature conditions (Geisler et al., 2003a, 2007). Overall, these studies collectively support the idea that alteration processes in zircon can involve the interaction of fluids, the diffusion of elements, and structural changes. The presence of water and the diffusion of hydrous species play important roles in these alteration processes, which can lead to the formation of altered domains within zircon crystals.

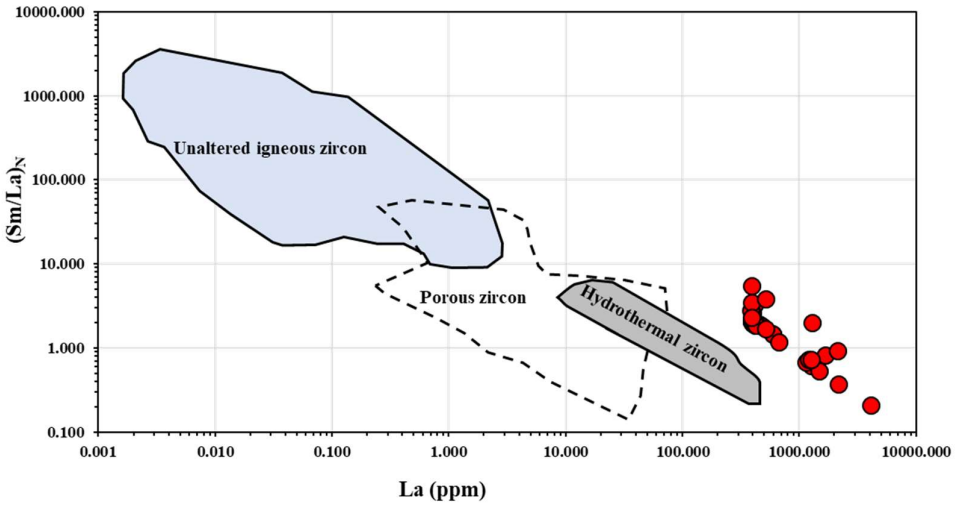

Figure 7. Chondrite-normalized Sm/La ratio vs. La (ppm) discrimination diagram (after Hoskin, 2005; Grimes et al., 2009; Bouvier et al., 2012) with zircons from granitoids of the Um Ara area.

The Um Ara zircon is far from the typical zircon in chemical composition and crystal structure. The total amount of major elements varies wildly, from 80% to almost 100%, with decreasing ZrO_2 and SiO_2 contents linearly with decreasing analytical totals (Figure 5a). Sums of cations in zircon analyses generally increase from around 2.002 to 2.098 apfu (atoms per formula unit) as the overall analytical total decreases from around 99 to 88 wt% (Table 2). This suggests that the calculated formulae with lower totals deviate from ideal zircon stoichiometry. The reasons of these deficiencies in microprobe results are still debated, but several hypotheses have been proposed: 1) the presence of water and hydroxyl groups degrade the mineral under the electron beam (Tornroos, 1985; Smith et al., 1991; Geisler et al., 2003a); 2) presence of numerous micropores and voids or structural vacancies (Pointer et al., 1988, Kempe et al., 2000; Nasdala et al., 2009); and 3) charge-compensating oxygen defects associated with divalent and trivalent cations, such as Ca, Fe, and REE (Perez-Soba et al., 2007). Generally, there is no consensus on the primary cause(s) of the low analytical totals, and it may involve a combination of these factors. However, the Um Ara zircons contain unusually high and variable amounts of elements not typically found in their crystal structure. Notably, the concentrations of REEs, U, and Th can be extreme, exceeding 2 wt%, 7 wt%, and 9 wt%, respectively.

 doi:10.20944/preprints202407.1284.v1

In comparison, even the most enriched igneous zircons typically contain only around 1 wt% REEs and less than 3 wt% U and Th (Hoskin and Schaltegger, 2003; Kirkland et al., 2015).

The alteration process of the Um Ara zircon begins with a leaching stage, where hydrothermal fluids react with the zircon grains and dissolve certain elements from the crystal structure. Zr and Si are particularly susceptible to this leaching, resulting in their removal from the zircon. As the leaching progresses, voids or altered remnants are left behind within the zircon grains. The hydrothermal fluids, become enriched with elements such as U, Th, Hf, Fe, Al, Ca, Ti, P, Y, As, and REEs, then infiltrate these void spaces. This observed alteration process is consistent with the findings reported by Geisler et al. (2003), who investigated the chemical and structural changes in metamict zircon crystals from the Gabel Hamradom in the Egyptian Eastern Desert. They found that the metamict, U- and Th-rich areas of the zircon exhibited significant enrichment in elements like Ca, Al, Fe, Mn, light REEs, and water species while experiencing the depletion of Zr, Si, and radiogenic lead (Pb). Geisler et al. (2003) attributed these chemical changes to an intensive reaction with a low-temperature aqueous solution, with temperatures varying from 120 to 200 °C. The presence of this aqueous solution facilitated the alteration process, leading to the enrichment of certain elements and the loss of others within the metamict zircon domains.

The negative correlation observed between ZrO_2 and elements such as ThO_2, UO_2, and Hf suggests a simple substitution mechanism (Figure 8a–c): (Th^{4+}, U^{4+}) = Zr^{4+}; Hf^{4+} = Zr^{4+} (Frondel, 1953). This implies that these elements replace Zr in the zircon structure, where their effective ionic size and charge are compatible with the crystal lattice. The suggestion made by Finch and Hanchar (2003) regarding the incorporation of $(UO_2)^{2+}$ into the zircon lattice at octahedral interstitial positions is an important insight into the crystal-chemical considerations of zircon alteration. This implies that the $(UO_2)^{2+}$ molecular group could potentially be incorporated into the altered zircon variety during the alteration process. In addition to the incorporation of $(UO_2)^{2+}$, the chemistry of zircon supports the possibility of the formation of secondary minerals such as uranophane. Uranophane commonly appears as distinct nano- and micro-inclusions within the zircon or at its peripheries (Figure 2d). The presence of uranophane, xenotime, thorite, and apatite inclusions within zircon suggests that the alteration process involves the interaction of aqueous fluids carrying U, Th, Ca, P, and REEs.

In addition to the previous simple substitution, trivalent rare earth elements (REEs) and yttrium (Y) can also substitute for Zr^{4+} (Figure 8d), while pentavalent phosphorus (P) can substitute for Si^{4+}, according to coupled substitution ($(Y, REE)^{3+} + P^{5+} = Zr^{4+} + Si^{4+}$, Speer 1982). However, it has been observed that trivalent REEs are typically more abundant than P in natural zircons on an atomic basis. This suggests that additional elements must participate in balancing the trivalent REEs in the zircon structure. Hoskin et al. (2000) proposed that interstitial elements such as Mg^{2+}, Fe^{2+}, Fe^{3+}, and Al^{3+} could offer charge stability for REE replacement beyond what is allowed by P replacement. They proposed two "xenotime-type" reactions, as shown in Figure (8e-f), to explain this charge balancing. The first reaction involves $(Al, Fe)^{3+} + 4(Y, REE)^{3+} + P^{5+} = 4Zr^{4+} + Si^{4+}$, while the second reaction involves $(Mg, Fe)^{2+} + 3(Y, REE)^{3+} + P^{5+} = 3Zr^{4+} + Si^{4+}$. Furthermore, the combination of water and hydroxyl into parental zircon is probable through the reaction $(Mn^{+} + n(OH)^{-} + (4–n)H_2O = Zr^{4+} + (SiO_4)^{4-}$, where *M* is a metal cation and *n* is an integer (Caruba and Iacconi, 1983). This suggests that water and hydroxyl groups can be integrated into the zircon structure by replacing Zr and Si.

The alteration processes significantly affect the distribution pattern of REEs in the parental zircon. The altered zircon exhibits distinct fractionation behavior compared to unaltered magmatic zircon, as shown in Figure 6. The irregular chondrite-normalized REE patterns observed in altered zircon may indicate a selective substitution of specific REEs within the crystal lattice of the mineral. This suggests that certain REEs are preferentially incorporated into the zircon structure during the alteration process.

Analysis of the Um Ara zircons reveals several key features that contradict a primary igneous origin as described by Hoskin and Schaltegger (2003). These zircons exhibit high and variable levels of elements not typically found in their crystal structure (often referred to as "non-formula" elements). Additionally, they have low concentrations of SiO_2 and ZrO_2. These characteristics are instead characteristic of zircons that have undergone metamictization or radiation damage (Geisler,

 doi:10.20944/preprints202407.1284.v1

2002; Geisler et al., 2005; Marsellos & Garver, 2010). This conclusion is supported by the BSE images of the Um Ara zircons that reveal textural evidence of extensive radiation damage. This damage manifests as voids, fractures, and highly porous regions throughout the zircon grains, with features ranging from micrometer to nanometer in size (Figure 2).

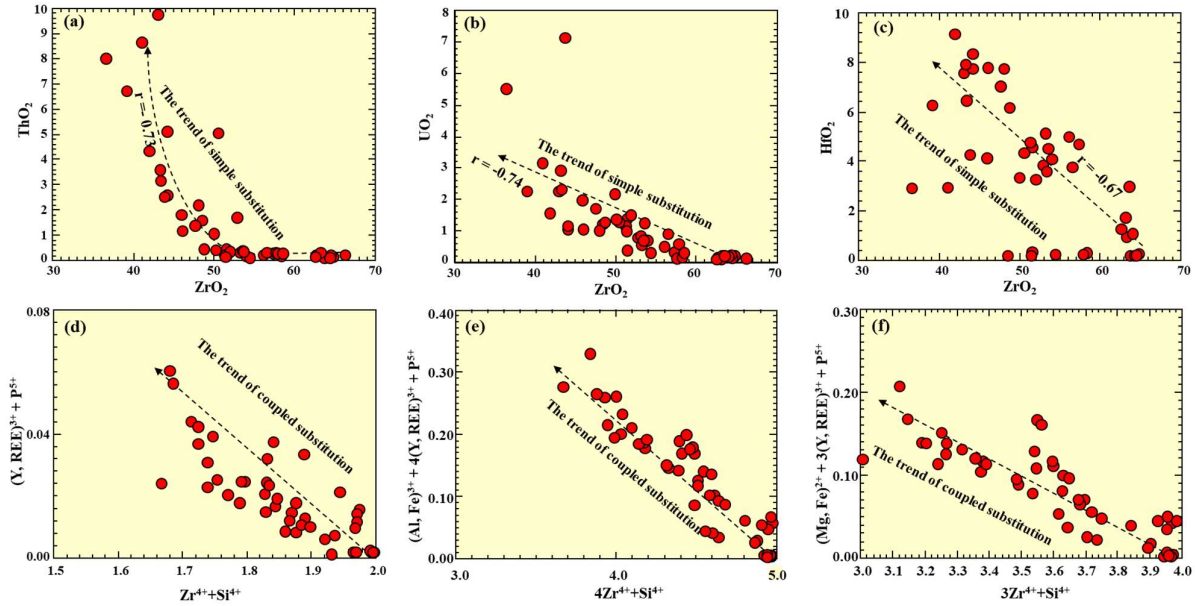

Figure 8. Dominant simple and coupled substitution in zircon from the Um Ara granite: **(a)** ZrO_2 vs. ThO_2; **(b)** ZrO_2 vs. UO_2; **(c)** ZrO_2 vs. HfO_2; **(d)** $(Y, REE)^{3+} + P^{5+}$ vs. $Zr^{4+}+Si^{4+}$; **(e)** $(Al, Fe)^{3+} + 4(Y, REE)^{3+} + P^{5+}$ vs. $4Zr^{4+}+Si^{4+}$; **(f)** $(Mg, Fe)^{2+} + 3(Y, REE)^{3+} + P^{5+}$ vs. $3Zr^{4+}+Si^{4+}$. Negative correlations in these diagrams indicate that Th, U, Hf, Al, Fe, Mg, P, Y, and REE were incorporated in the parental zircon at the expense of Zr and Si, leading to the non-formula elements uptake of the Um Ara altered zircon.

The accommodation of non-formula elements in metamict zircon can occur through a dissolution-reprecipitation mechanism, where the porous, damaged structure of metamict zircons facilitates the dissolution of the zircon lattice. This allows non-formula elements to be incorporated during the reprecipitation of the zircon. The porous 'sponge-like' texture observed in the Um Ara zircon supports this mechanism (Figure 2b). Diffusion-reaction mechanism could also play a role in the absorption of non-formula elements, where these elements can diffuse into the radiation-damaged parts of the zircon structure. Chemical reactions then incorporate these elements into the zircon. Regardless of the exact mechanism, the key point is that this elemental uptake will significantly obscure and alter the primary chemical composition of the zircon. The original igneous signature is overprinted by these secondary alteration processes.

5.2. Timing of 'Non-Formula' Element Uptake in Um Ara Zircon

The granitic masses of the Um Ara area formed millions of years ago (between 620 and 530 Ma ago) after a period of intense orogenic activity. This dating is confirmed by studies on zircon crystals from these granites, which show a crystallization age of 603±14 Ma (Moussa et al., 2007). The intrusion of these granites seems to be influenced by deep shear zones and faulting in the Earth's crust. These shear zones acted as pathways for rare metals-bearing hydrothermal fluids. The granites contain various accessory minerals, like columbite, ilmenite, zircon, xenotime, thorite, monazite, and apatite. These minerals behave differently when they are altered by fluids. Some zircon crystals have compositions close to ideal stoichiometry, while others show signs of alteration. Normally, elements like uranium, thorium, and REEs wouldn't be easily incorporated into zircon crystals, especially at low temperatures. So, it's likely that something changed the zircon crystals (metamictization) to allow them to accommodate these elements.

 doi:10.20944/preprints202407.1284.v1

There are two possibilities for elemental uptake during the geological history of the Um Ara zircons: (i) a high-temperature hydrothermal event associated with the main rifting phase of the Red Sea (ca. 1.8 Ga) may have led to element uptake in the zircon. This is supported by previous study of hydrated, trace element-rich metamict zircons from the Egyptian Eastern Desert, as proposed by Geisler et al. (2003), and (ii) Low-temperature alteration by oxic groundwater, where the influence of groundwater on previously decomposed accessory minerals within the host granitic rocks may have led to element uptake in the zircon. The $^{230}Th/^{234}U$ ages of 50,000 to 159,000 years for uranophane from the Um Ara granites have been obtained by Dawood (2001). This timeframe matches up with periods of heavy rainfall (pluvial periods) known as the Kubbaniyan and Nabtian that occurred in the Egyptian Eastern Desert. A similar low-temperature weathering event has been suggested as a mechanism for element uptake in metamict zircons, as documented by studies of Delattre et al. (2007) and Hay and Dempster (2009).

6. Conclusions

The EPMA data and compositional analysis provide valuable insights into the elemental and mineralogical changes that occurred during the alteration of zircon. The zircon from the Um Ara alkali-feldspar granites exhibits high concentrations of non-formula elements such as U, Th, Hf, REEs, P, Al, Ca, Fe, and Ti. They also display extensive structural features indicative of radiation damage, including porous and amorphous domains, cavities, and voids. These characteristics are consistent with the zircon undergoing significant hydrothermal alteration following their initial crystallization. The observed textures and presence of both simple and coupled substitutions suggest that the alteration occurred through coupled dissolution-reprecipitation processes influenced by aqueous fluids. Negative correlations between Zr and the non-formula elements indicate that these elements were incorporated into zircon at the expense of Zr and Si. The alteration processes have significantly affected the distribution and fractionation of REEs in the original zircon, leading to distinct REE patterns and anomalies.

Based on the presented mineralogical and geochemical data, as well as the current literature knowledge, I can summarize the sequence of events that led to zircon alteration and high concentrations of non-formula element contents: (1) Initial zircon crystallization around 603 Ma in the Um Ara granitic source. (2) A major hydrothermal event, contemporaneous with the rifting of the Red Sea around 1.8 Ga, led to the breakdown of accessory minerals like xenotime, thorite, monazite, and apatite. The released U, Th, P, Ca, Al, Fe, and REEs were then incorporated into the metamict zircon structures as non-formula elements. (3) Subsequent pluvial periods in the Kubbaniyan and Nabtian periods (around 50,000-159,000 years ago) may have allowed further uptake of non-formula elements during low-temperature alteration. The shear zones within Um Ara granites facilitated the mobilization and transport of non-formula elements-bearing fluids, likely as carbonate and fluoride complexes. The interplay between hydrothermal fluids, meteoric water, and the shear zone environments appears to have been a key driver for the uptake of the non-formula elements into the altered zircon.

Funding: This research work was funded by Institutional Fund Projects under grant no. (IFPIP-1441-145-1443).

Data Availability Statement: The data presented in this study are contained within the article.

Acknowledgments: The authors gratefully acknowledge technical and financial support from the Ministry of Education and King Abdulaziz University, Jeddah, Saudi Arabia. The Faculty of Earth Sciences, King Abdulaziz University, KSA, is acknowledged for using their mineral separation machine and EPMA facilities.

Conflicts of Interest: The author declares no conflict of interest.

References

1. Abd El-Naby, H. High and low temperature alteration of uranium and thorium minerals, Um Ara granites, south Eastern Desert, Egypt. *Ore Geol. Rev.* **2009**, 35, 436–446.

2. Abdalla, H.M.; Ishihara, S.; Matsueda, H.; Abdel-Monem, A.A. On the albite-enriched granitoids at Um Ara area, Southeastern Desert, Egypt. 1. Geochemical, ore potentiality and fluid inclusion studies. *J. Geochem. Explor.* **1996**, 57, 127–138.
3. Bouvier, A.-S.; Ushikubo, T.; Kita, N.T.; Cavoise, A.J.; Kozdon, R.; Valley, J.W. Isotopes and trace elements as a petrogenetic tracer in zircon: insights from Archean TTGs and sanukitoids. *Contrib Mineral Petrol* **2012,** 163, 745–768.
4. Caruba, R.; Iacconi, P. Les zircons de Narssârssuk (Groënland) - L'eau et les groupements OH dans les zircons métamictes. *Chem Geol* **1983**, 38, 75–92.
5. Claiborne, Lily.L.; Miller, C.F.; Wooden, J.L. Trace element composition of igneous zircon: a thermal and compositional record of the accumulation and evolution of a large silicic batholith, Spirit Mountain, Nevada. *Contrib Mineral Petrol* **2010**, 160, 511–531.
6. Dawood, Y.H. Uranium-series disequilibrium dating of secondary uranium ore from south Eastern Desert of Egypt. *Appl Radiat Isot* **2001**, 881–887.
7. Delattre, S.; Utsunomiya, S.; Ewing, R. C.; Boeglin, J.-L.; Braun, J.; Balan, E.; Calas, G. Dissolution of radiation-damaged zircon in lateritic soils. *Amer Miner* **2007**, 92, 1978–1989. https://doi.org/10.2138/am.2007.2514.
8. Ewing, R.C.; Meldrum, A.; Wang, L.; Weber, W.J.; Corrales, L.R. Radiation effects in zircon. *Rev. Mineral. Geochem.* **2003**, 53, 387–425. https://doi.org/10.2113/0530387.
9. Frondel, C. Hydroxyl substitution in thorite and zircon. *Amer Miner* **1953**, 38,1007–1018.
10. Geisler, T.; Schaltegger, U.; Tomaschek, F. Re-equilibration of zircon in aqueous fluids and melts. *Elements* **2007**, 3, 43–50.
11. Geisler, T.; Burakov, B.E.; Zirlin, V.; Nikolaeva, L.; Pöml, P. A Raman spectroscopic study of high-uranium zircon from the Chernobyl "lava". *European Journal of Mineralogy* **2005**, 17, 883–894.
12. Geisler, T.; Rashwan, A.A.; Rahn, M.K.W.; Poller, U.; Zwingmann, H.; Pidgeon, R.T.; Schleicher, H.; Tomaschek, F. Low-temperature hydrothermal alteration of natural metamict zircons from the Eastern Desert, Egypt. *Mineralogical Magazine* **2003**, 67, 485–508.
13. Geisler, T.; Pidgeon, R.T.; Kurtz, R.; van Bronswijk, W.; Schleicher, H. Experimental hydrothermal alteration of partially metamict zircon. *Amer Miner* **2003a**, 86, 1496–1518.
14. Geisler, T. Isothermal annealing of partially metamict zircon: evidence or a three-stage recovery process. *Physics and Chemistry of Minerals* **2002**, 29, 420–429.
15. Grimes, C.B.; John, B.E.; Cheadle, M.J.; Mazdab, F.K.; Wooden, J.L.; Swapp, S.; Schwartz, J.J. On the occurrence, trace element geochemistry, and crystallization history of zircon from in situ ocean lithosphere. *Contrib Mineral Petrol* **2009**, 158, 757–783.
16. Finch, R.J.; Hanchar, J.M. Structure and chemistry of zircon and zircon-group minerals. *Rev. Mineral. Geochem.* **2003**, 53, 1–25.
17. Harlov, D.E.; Anczkiewicz, R.; Dunkley, D.J. Metasomatic alteration of zircon at lower crustal P-T conditions utilizing alkali- and F-bearing fluids: Trace element incorporation, depletion, and resetting the zircon geochronometer. *Geochimica et Cosmochimica Acta* **2023**, 352. DOI: 10.1016/j.gca.2023.05.011.
18. Hay, D.C.; Dempster, T.J. Zircon behaviour during low-temperature metamorphism. *J. Petrol.* **2009**, 50, 571–589.
19. Hoskin, P.W.O. Trace-element composition of hydrothermal zircon and the alteration of Hadean zircon from the Jack Hills, Australia. *Geochim. Cosmochim. Acta* **2005**, 69, 637–648.
20. Hoskin, P.W.O.; Kinny, P.D.; Wyborn, D.; Chappell, B.W. Identifying accessory mineral saturation during differentiation in granitoid magmas: an integrated approach. *Journal of Petrology* **2000**, 41, 1365–1396.
21. Hoskin, P.W.O.; Schaltegger, U. The composition of zircon and igneous and metamorphic petrogenesis. *Reviews in Mineralogy and Geochemistry* **2003**, 53, 27–62.
22. Kempe, D.; Gruner, T.; Nasdala, L.; Wolf, D. Relevance of cathodoluminescence for the interpretation of U-Pb zircon ages, with an example of an application to a study of zircons from the Saxonian Granulite Complex, Germany. In *Cathodoluminescence in Geosciences*; Pagel, M.; Barbin, V.; Blanc, P.; Ohnenstetter, D., Eds., Springer, Berlin, Heidelberg, New York, 2000, pp. 415–455.
23. Kirkland, C.; Smithies, R.; Taylor, R.; Evans, N.; McDonald, B. Zircon Th/U ratios in magmatic environs. *Lithos* **2015**, 212, 397–414. https://doi.org/10.1016/j.
24. Lenting, C.; Geisler, T.; Gerdes, A.; Kooijman, E.; Scherer, E.E.; Zeh, A. The behavior of the Hf isotope system in radiation damaged zircon during experimental hydrothermal alteration. *Amer Miner* **2010**, 95, 1343–1348.
25. Lewerentz, A.; Harlov, D.E.; Scherstén, A.; Whitehouse, M.J. Baddeleyite formation in zircon by Ca-bearing fluids in silica-saturated systems in nature and experiment: resetting of the U–Pb geochronometer. *Contrib Mineral Petrol* **2019**, 174, 64. 10.1007/s00410-019-1600-8.
26. Marsellos, A.E.; Garver, J.I. Radiation damage and uranium concentration in zircon as assessed by Raman spectroscopy and neutron irradiation. *Amer Miner* **2010**, 95, 1192–1201.

27. Moussa, E.M.; Stern, R.J.; Manton, W.I.; Ali, K.A. SHRIMP zircon dating and Sm/Nd isotopic investigations of Neoproterozoic granitoids, Eastern Desert, Egypt. *Precambr Res* **2007**, 160, 341–356.
28. Murakami, T.; Chakoumakos, B.C.; Ewing, R.C.; Lumpkin, G.R.; Weber, W.J. Alpha-decay event damage in zircon. *Amer Miner* 1991, 76, 1510–1532.
29. Nasdala, L.; Kronz, A.; Wirth, R.; Váczi, T.; Pérez-Soba, C.; Willner, A.; Kennedy, A.K. The phenomenon of deficient electron microprobe totals in radiation-damaged and altered zircon. *Geochim Cosmochim Acta* **2009**, 73, 1637–1650.
30. Pérez -Soba, C.; Villaseca C.; Del Tánago, J.G; Nasdala, L. The composition of zircon in the peraluminous Hercynian granites of the Spanish Central System batholith. *Canad Mineral* **2007**. 45, 509–527.
31. Pointer, C.M.; Ashworth, J.R.; Ixer, R.A. The zircon-thorite mineral group in metasomatized granite, Ririwai, Nigeria 1. Zoning, alteration and exsolution in zircon. *Mineral Petrol* **1988,** 39, 21–37.
32. Reddy, S.M.; Timms, N.; Kinny, P.D.; Buchan, C.; Trimby, P.; Blake, K. Crystal-plastic deformation of zircon: a defect in the assumption of chemical robustness. *Geology* **2006**, 34, 257–260. https://doi.org/10.1130/G22110.1.
33. Scott, V.D.; Love, G.; Reed S.J.B. Quantitative Electron-Probe Microanalysis (2nd edition). Ellis Horwood. London and New York, 1995, 311p.
34. Seydoux-Guillaume, A.M.; Bingen, B.; Paquette, J.L.; Bosse, V. Nanoscale evidence for uranium mobility in zircon and the discordance of U-Pb chronometers. *Earth Planet Sc Lett* **2015**, 409, 43–48.
35. Skublov, S.G.; Berezin, A.V.; Li, X.-H.; Li, Q.-L.; Salimgaraeva, L.I.; Travin, V.V.; Rezvukhin, D.I. Zircons from a Pegmatite Cutting Eclogite (Gridino, Belomorian Mobile Belt): U-Pb-O and Trace Element Constraints on Eclogite Metamorphism and Fluid Activity. *Geosciences* **2020**, 10, 197. https://doi.org/10.3390/geosciences 10050197
36. Smith D.G.W.; de St. Jorre L.; Reed S J.B.; Long J.V.P. Zonally metamictized and other zircons from Thor Lake, Northwest Territories. *Canad Mineral* **1991**. 29, 301–309.
37. Soman, A.; Geisler, T.; Tomaschek, F.; Grange, M.; Berndt, J. Alteration of crystalline zircon solid solutions: A case study on zircon from an alkaline pegmatite from Zomba-Malosa, Malawi. *Contrib Mineral Petr* **2010**, 160, 909–930.
38. Speer, J.A. Zircon. Mineralogical Society of America, *Rev. Mineral.* **1982**, 5, 67– l12.
39. Tomaschek, F.; Kennedy, A.K.; Villa, I.M.; Lagos, M.; Ballhaus, C. Zircons from Syros, Cyclades, Greece—recrystallization and mobilization of zircon during high-pressure metamorphism. *J Petrol* **2003**, 44, 1977–2002.
40. Törnroos, R. Metamict zircon from Mozambique. *Bull. Geol. Soc. Finland* **1985,** 57, 181–195.
41. Trail, D.; Watson, E.B.; Tailby N.D. Ce and Eu anomalies in zircon as proxies for the oxidation state of magmas. *Geochim Cosmochim Acta* **2012**, 97, 70–87.